

Dynamics of subsurface oxygen formation in catalytic water formation on a Rh(1 1 1) surface — experiment and simulation

M.I. Monine^a, A. Schaak^b, B.Y. Rubinstein^a, R. Imbihl^{b,*}, L.M. Pismen^a

^a Department of Chemical Engineering, Technion, Haifa, Israel

^b Institut für Physikalische Chemie und Elektrochemie, Universität Hannover, Callinstr. 3-3a, 30167 Hannover, Germany

Abstract

The catalytic $O_2 + H_2$ reaction on Rh(1 1 1) has been investigated in the 10^{-6} – 10^{-5} mbar range using photoelectron emission microscopy as spatially resolving method. While the reaction without pretreatment of the sample displays simple bistable behavior, we find that after extended pre-oxidation of the sample ($p_{O_2} = 2 \times 10^{-4}$ mbar, $T = 770$ K, $t_{OX} > 24$ h), low work function (LWF) areas develop dynamically in the collision of reaction fronts. The LWF areas have been assigned to subsurface oxygen. We present a simple three-variable model which reproduces the formation of LWF areas in the collision of reaction fronts. © 2001 Elsevier Science B.V. All rights reserved.

Keywords: Subsurface oxygen formation; Low work function; Photoelectron emission microscopy

1. Introduction

Chemical waves on surfaces are usually considered as strictly 2D reaction–diffusion systems [1,2] but in a number of cases this assumption does not hold as demonstrated in recent years with reaction systems involving oxygen dissolved in the bulk [3–12]. A so-called subsurface oxygen (sub-O) species located presumably directly underneath the surface plane takes part in pattern formation as shown for a number of systems, Pt(1 0 0)/CO + O₂ [4,5], Pt(1 1 0)/CO + O₂ [6–8] and Rh(1 1 1)/NO + H₂ [9,10]. In photoelectron emission microscopy (PEEM), bright areas indicating a reduced work function (WF) dynamically form and disappear as reaction fronts or pulses interact on the surface. These low work function (LWF)

areas have been assigned to sub-O based on the argument that the oxygen underneath the surface plane exhibits a negative dipole moment thus lowering the WF. In catalytic CO oxidation on Pt(1 1 0), the formation of the sub-O species has been linked to the mass transport of Pt atoms associated with the $1 \times 1 \leftrightarrow 1 \times 2$ phase transition [6–8]. However, the formation of LWF areas has also been observed on Rh(1 1 1) which is a structurally stable surface. The question whether a common mechanism for sub-O formation exists in all the above-mentioned pattern forming systems remains therefore open. Here we present experiments together with a mathematical simulation for the formation of sub-O in a rather simple reaction, the $O_2 + H_2$ reaction on Rh(1 1 1) [11,12]. The formation of a sub-O species on Rh(1 1 1) has already been found in the chemically more complex system Rh(1 1 1)/NO + H₂. The system studied here can be considered in a way as a less complex subset of the Rh(1 1 1)/NO + H₂ system. The formation of sub-O in the system Rh(1 1 1)/O has been the subject of several studies including molecular

* Corresponding author. Tel.: +49-511-762-2349;
fax: +49-511-762-4009.
E-mail address: ronald.imbihl@mbx.pci.uni-hannover.de
(R. Imbihl).

beam experiments [13,14] and photoelectron diffraction [15]. Oscillatory and chemical wave patterns have been found in the $\text{NO} + \text{H}_2$ reaction on $\text{Rh}(111)$ [9,12,16]. The $\text{O}_2 + \text{H}_2$ reaction on $\text{Rh}(111)$ exhibits usually simple bistable behavior but after exposure to a large dose of oxygen (10^5 L) a rather unusual behavior was observed. Triangularly shaped reaction fronts appeared in the titration with hydrogen which is of course in contrast to the isotropic propagation one should expect on an f.c.c. (111) surface [12]. The unusual behavior can clearly be traced back to the presence of a substantial concentration of oxygen in the bulk. The oxygen pretreatment is also responsible for another type of unusual behavior demonstrated in this paper.

2. Experimental observations

We study the reaction in a standard UHV system under low pressure conditions ($p < 10^{-4}$ mbar), so

that we can neglect temperature changes which could arise due to the exothermicity of the reaction. For spatially resolved measurements, we employ PEEM. This method images with a resolution of roughly $1 \mu\text{m}$ primarily the local WF and is therefore sensitive to changes in the adsorbate layer. Chemisorbed oxygen which increases the WF is accordingly imaged as dark area whereas adsorbates which decrease the WF appear as bright areas in PEEM. We observe the formation of LWF areas only when we expose the $\text{Rh}(111)$ sample prior to the actual experiment to a large dose of oxygen [11]. This is accomplished here by exposing the sample to oxygen at $p_{\text{O}_2} = 2 \times 10^{-4}$ mbar and $T = 770 \text{ K}$ for more than 36 h. The chemisorbed oxygen is then removed by short exposure to H_2 at $T = 450 \text{ K}$ and $p_{\text{H}_2} = 2 \times 10^{-7}$ mbar until the (1×1) pattern of the clean surface is present in LEED. After that we dose some oxygen onto the surface, so that a layer of chemisorbed oxygen forms, and titrate this oxygen layer with hydrogen. Reaction fronts develop,

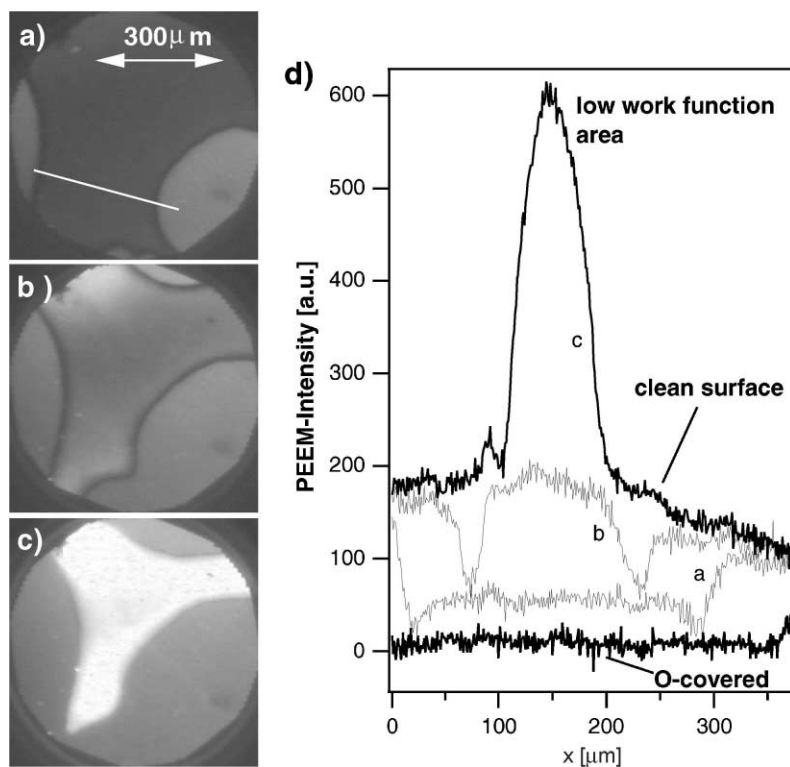


Fig. 1. Formation of low WF areas upon titration of an oxygen-covered surface with hydrogen. Experimental conditions: $t_{\text{O}_2} = 40 \text{ h}$, 160 L O_2 exposure, $T = 450 \text{ K}$, $p_{\text{H}_2} = 4 \times 10^{-7}$ mbar. (a)–(c) PEEM images showing the development of a low WF area. Time between frames is 10 s. (d) PEEM intensity profiles taken along the white line indicated in (a).

as it is also the case without the oxygen pretreatment, but upon collision of the fronts a new species develops. The PEEM images in Fig. 1 show how reaction fronts coming from different directions all collide in a central area. When the oxygen-covered area becomes smaller and smaller, the area enclosed by the fronts starts to brighten (Fig. 1b). The intensity reaches a very high level, until, finally, with the collision of the fronts the LWF area is extinguished and the intensity returns to the initial gray level.

A calibration of the intensity in the system Rh(111)/NO + H₂ displaying similar behavior revealed that the highest intensity level reached there corresponds to a WF which is 0.8 eV below the level of the clean surface [10]. Some details of the PEEM images should not be overlooked. As shown in Fig. 1b, dark bands form at the reaction front which later on vanish when the intensity of the LWF area reaches a very high level (Fig. 1c). The change in brightness and in the front velocity can best be seen in a 1D $x-t$ plot of the PEEM intensity displayed in Fig. 2.

Below a distance of 150 μm , the brightness of the oxygen-covered area starts to increase until, after collision, the surface returns to initial gray level. The LWF areas in these experiments have been assigned to sub-O based on the following arguments: (i) a lowering of the WF is consistent with the assumed location of this species underneath the surface plane, (ii) the necessary pretreatment with oxygen can be explained

if we assume that a certain oxygen concentration in the bulk is required to prevent the diffusion of the sub-O species into the deeper layers of the Rh bulk, and (iii) the analogy with CO oxidation on Pt(100) and Pt(110) where a rather similar behavior is observed with PEEM and where the LWF areas have been associated with sub-O [4,5]. The adsorption properties and the reactivity of an area with sub-O are demonstrated in the following experiments depicted in Fig. 3.

When we prepare a sub-O island in a titration experiment and then expose it to oxygen, the whole surface becomes uniformly dark due to formation of a layer of chemisorbed oxygen. This is demonstrated in Fig. 3b showing the PEEM intensity variation at various selected spots of the surface. Oxygen can apparently adsorb on top of a sub-O layer but, as can be seen from the time needed for saturation, the sticking coefficient is slightly reduced. Titration of the oxygen-covered surface with hydrogen first removes the chemisorbed oxygen layer restoring the sub-O island and only in a second step is then the sub-O species reacted away. The local PEEM intensity in Fig. 3c and the intensity profiles in Fig. 3d show that the reactive removal of the sub-O layer proceeds via a propagating front. A rather unusual behavior can be observed upon extending the oxygen pretreatment to 60 h. As demonstrated by the sequence of PEEM images in Fig. 4, immediately after the collision of two circular reaction fronts secondary fronts nucleate in the collision

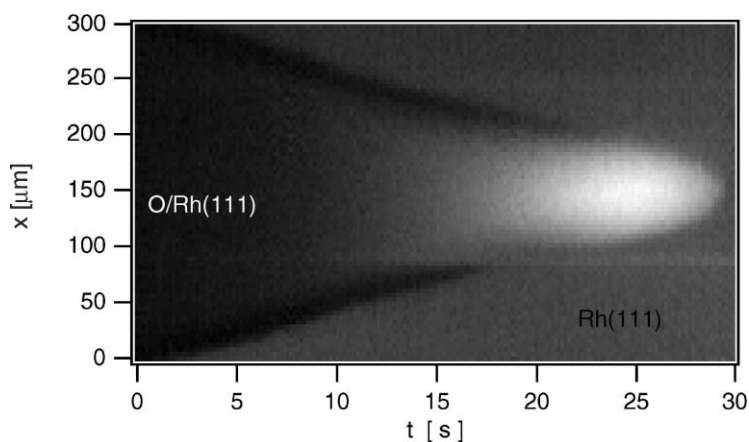


Fig. 2. $x-t$ diagram demonstrating how the formation of a low WF area between two colliding fronts leads to reduction of the front velocity. The $x-t$ diagram was constructed by taking PEEM intensity profiles in a direction perpendicular to the front line. Experimental conditions as in Fig. 1.

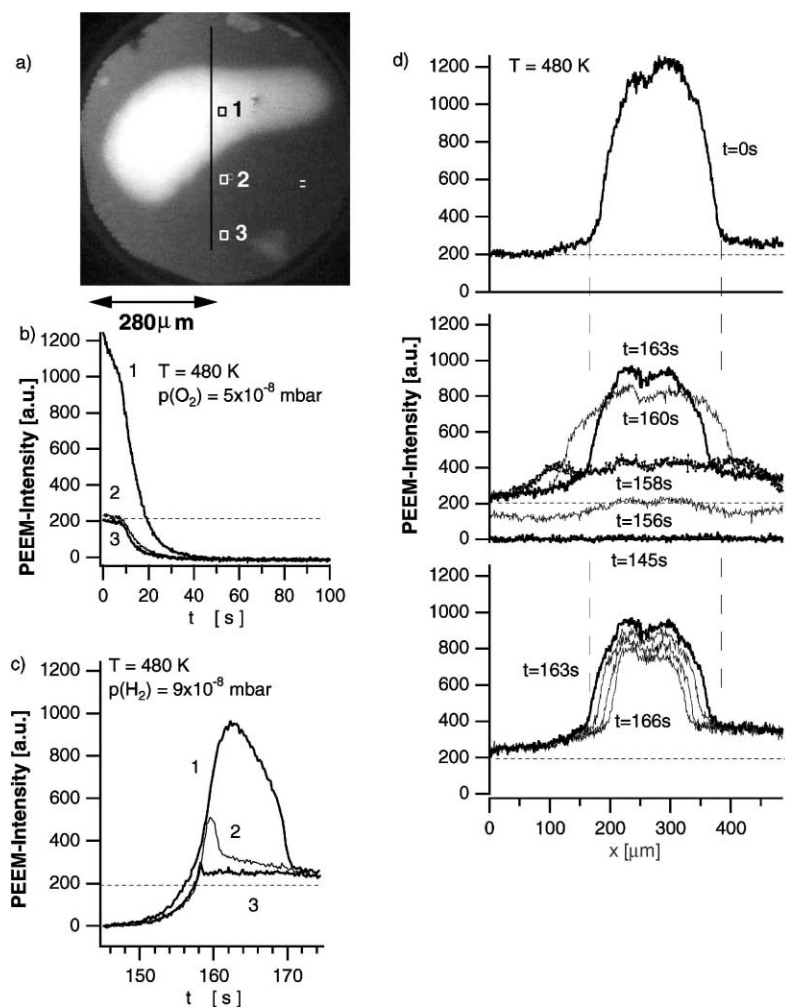


Fig. 3. Adsorption properties and reactivity of low WF areas. The low WF spot had been prepared through a titration experiment with 230L oxygen exposure, $T = 450$ K and $p_{\text{H}_2} = 2 \times 10^{-7}$ mbar: (a) PEEM image showing the low WF spot together with three square windows inside which the digitized intensity was integrated. Along the vertical line intensity profiles were taken. (b) Local PEEM intensity variation during O₂ adsorption at the three selected square windows displayed in (a). (c) Local PEEM intensity variation during titration of the oxygen which has been adsorbed in (b) with hydrogen. (d) PEEM intensity profiles showing the spatial evolution of the PEEM intensity during the O₂ adsorption experiment of (b) and the titration with H₂ in (c).

area, propagating from there backwards into the area where chemisorbed oxygen has just been removed by the primary fronts.

These secondary fronts cause a transition of the surface to a brighter gray level in PEEM. The velocity of these secondary fronts is initially much higher than that of the primary fronts but shortly after covering a certain distance they slow down and eventually come

to a rest (Fig. 4d). The sequence of PEEM images in Fig. 4d–f demonstrates how subsequently several of these secondary reaction fronts are generated as primary reaction fronts coming from various directions collide in the imaged area. The contrast before and after the secondary front increases with longer duration of the oxygen pretreatment suggesting the following tentative explanation. The primary reaction front

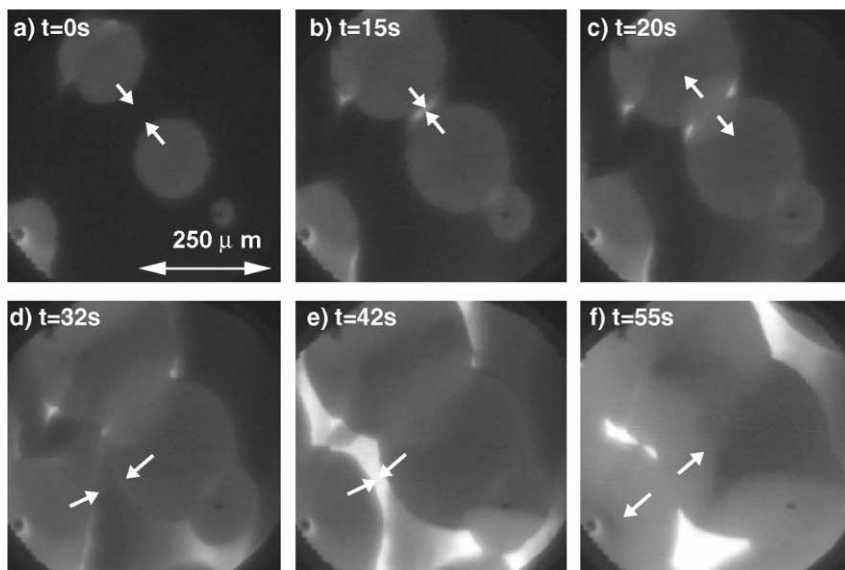


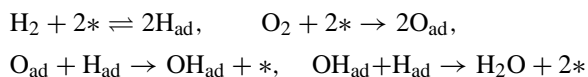
Fig. 4. PEEM images showing the formation of secondary reaction fronts after very long oxygen pretreatments with $t_{OX} = 62$ h. The secondary fronts emanate from the area where two primary fronts collide and they propagate from there in the backward direction. Experimental conditions: $T = 450$ K, $p_{O_2} = 2 \times 10^{-6}$ mbar and $p_{H_2} = 4.6 \times 10^{-6}$ mbar.

removes chemisorbed oxygen but it does not lead to a complete depletion of oxygen in the subsurface region. If, therefore, after the passage of the primary front oxygen from the bulk segregates to the subsurface region and from there to the surface enough chemisorbed oxygen should soon be available to feed the propagation of a secondary front.

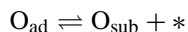
3. Simulation

3.1. The model

The reaction between H_2 and O_2 proceeds via the steps of a Langmuir–Hinshelwood (LH) mechanism [17,18]:



to which we add the reversible formation of subsurface oxygen (O_{sub})



In molecular beam experiments with Rh(1 1 1)/O, Peterlinz and Sibener [14] determined the energy difference between subsurface sites and the energetically more favorable surface sites as 18 kJ mol^{-1} . If we restrict diffusion into the bulk to just one layer, the subsurface sites, we obtain the energy difference diagram displayed in Fig. 5.

The PEEM images (Fig. 1) demonstrated that the area between two colliding fronts already starts to brighten when the fronts are still $150 \mu\text{m}$ apart. This long-range interaction is apparently transmitted via diffusing hydrogen on the surface whose diffusion parameters provide the right length scale [19,20]. Furthermore, we have to assume that co-adsorbed hydrogen facilitates sub-O formation. Mechanistically, this may be caused by distortions of the substrate lattice thus lowering the activation barrier for diffusion into the bulk as indicated in Fig. 5. One arrives at the following set of three equations describing the variation in the oxygen and hydrogen coverages and in the subsurface concentration, c , with $0 < c < 1$:

$$\frac{\partial \theta_H}{\partial t} = k_1 p_{H_2} \theta_{H_2}^{ads} - k_2 \theta_H^2 - 2k_3 \theta_O \theta_H + D_H \nabla^2 \theta_H, \quad (1)$$

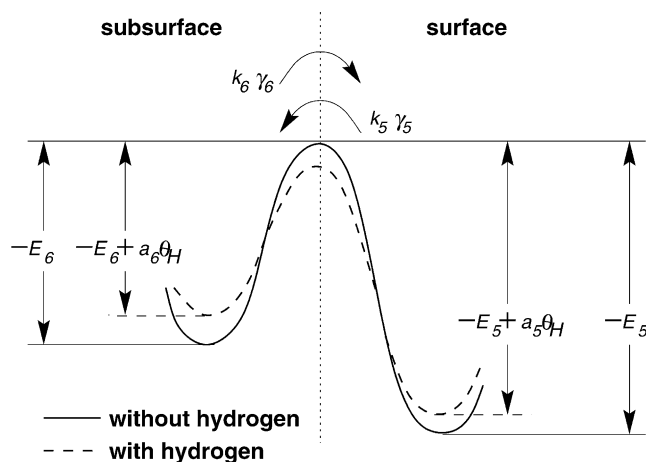


Fig. 5. Potential energy diagram.

$$\frac{\partial \theta_{\text{O}}}{\partial t} = k_4 p_{\text{O}_2} (1 - \theta_{\text{O}})^y - k_5 \gamma_5 \theta_{\text{O}} (1 - c) + k_6 \gamma_6 c (1 - \theta_{\text{O}}) - k_3 \theta_{\text{O}} \theta_{\text{H}}, \quad (2)$$

$$\frac{\partial c}{\partial t} = k_5 \gamma_5 \theta_{\text{O}} (1 - c) - k_6 \gamma_6 c (1 - \theta_{\text{O}}) \quad (3)$$

with

$$\theta_{\text{H}_2}^{\text{ads}} = \begin{cases} (\theta_{\text{H}_2}^*)^2, & \text{when } \theta_{\text{H}_2}^* > 0, \\ 0, & \text{when } \theta_{\text{H}_2}^* > 0, \end{cases}$$

and

$$\gamma_5 = \exp\left(\frac{a_5 \theta_{\text{H}}}{RT}\right), \quad \gamma_6 = \exp\left(\frac{a_6 \theta_{\text{H}}}{RT}\right).$$

The terms in the first two equations represent the various steps of the LH mechanism, i.e., the adsorption (k_1) and desorption (k_2) of hydrogen, the adsorption of oxygen (k_4), the surface reaction to form H_2O (k_3) and the surface diffusion of hydrogen (D_{H}). The third equation contains two terms representing oxygen diffusion into the bulk (k_5) and segregation of oxygen to the surface (k_6). For the catalytic $\text{O}_2 + \text{H}_2$ reaction, it has been demonstrated that the addition of the first H atom to chemisorbed oxygen is the slow step, whereas the subsequent H addition leading to H_2O is fast [18]. Accordingly, we can neglect the OH intermediate and formulate the rate of H_2O formation as given in Eqs. (1) and (2). Since the mobility of hydrogen is several orders of magnitude higher than that

of the more tightly bonded oxygen, we also neglect oxygen diffusion. Under typical reaction conditions, rapid desorption of hydrogen ensures a low hydrogen coverage (<1% of a monolayer). When we calculate the number of vacant sites available for H_2 adsorption, $\theta_{\text{H}_2}^*$, we can therefore neglect the hydrogen coverage:

$$\theta_{\text{H}_2}^* = 1 - \eta(\theta_{\text{O}} + \eta_c c),$$

where the constants η and η_c describe the site-blocking effect of chemisorbed oxygen and sub-O for H_2 adsorption. Sub-O cannot directly block an adsorption site but only through electronic effects, as it removes electron density from the Fermi level of the metal. For dissociative O_2 chemisorption, two adjacent vacant sites are required and this would correspond to $y = 2$ in Eq. (2). Often, however, the kinetics of O_2 adsorption does not obey this law and in our simulations we found that $y = 1$ yielded better quantitative agreement with the experimental data. The lowering of the energy barrier for oxygen diffusion by co-adsorbed hydrogen is described by two constants a_5 and a_6 in the model as indicated in Fig. 5. Two constants were chosen because interactions between the co-adsorbed species may have the effect that the energy barrier does not decrease by the same amount in both directions. In order to compare the simulation results with PEEM measurements, we calculate from the adsorbate coverages the WF which we simply approximate as

$$\text{WF} = \theta_{\text{O}} - c,$$

Table 1
Rates of the elementary steps in the Rh(1 1 1)/O₂ + H₂ reaction

k_i	Pre-exponential factor, v_i^0	E_i (kJ mol ⁻¹)	Reference
Hydrogen adsorption, k_1	4.5×10^5 ML s ⁻¹ mbar ⁻¹		[21]
Hydrogen desorption, k_2	2×10^{12} s ⁻¹	75	[22]
Water formation, k_3	10^6 s ⁻¹	28	[23]
Oxygen adsorption, k_4	1.36×10^5 ML s ⁻¹ mbar ⁻¹		[24]
O diffusion into bulk, k_5	6×10^4 s ⁻¹	54	[14]
O segregation, k_6	2×10^3 s ⁻¹	36	[14]
Hydrogen diffusion, D_H	26.8 cm ² s ⁻¹	38.15	[19]

i.e., we assume that the adsorbate complexes with chemisorbed oxygen and the sub-O species exhibit the same dipole moment but with opposite sign.

Table 1 lists the various constants used in the simulations. Other parameters are: $a_5 = 100 \times 10^3$ kJ/mol, $a_6 = 135 \times 10^3$ kJ/mol, $\eta = 1$ and $\eta_c = 2$.

The system of Eqs. (1)–(3) displays a usual bistable behavior in which the oxygen-rich state ($\theta_O = 1$, $c = 1$, $\theta_H = 0$) can be characterized as metastable and the oxygen-free one ($\theta_O \approx 0.05$, $c \approx 0.02$, $\theta_H \approx (4.0\text{--}40.0) \times 10^{-3}$, depending on p and T) is globally stable. A linear stability analysis shows that in the present p and T range, all eigenvalues are real. Moreover, $\lambda_{\max}^{\text{O-free}} < \lambda_{\max}^{\text{O-rich}} < 0$, where $\lambda_{\max}^{\text{O-rich}} = \text{const}$ and $\lambda_{\max}^{\text{O-free}}$ decreases with high p_{H_2} values. Therefore, we expect propagation of the O-free state as globally stable with a front speed increasing with p_{H_2} . It should be noted that a front connecting the two alternative states and the hydrogen diffusion are apparently essential for the formation of the low WF areas. We only get these low WF areas when a reaction and fronts are present but not in simple adsorption experiments and simulations. Nevertheless, the reason for the WF decrease is attributed to the reaction kinetics: the chemisorbed oxygen is removed by the reaction at the front, segregation of the sub-O to the surface is a slow process, thus the difference $\theta_O - c$ becomes negative (bright in PEEM).

In the numerical simulations, Eq. (1) has been transformed according to an implicit finite difference scheme and solved with the help of a tridiagonal matrix solver. Eqs. (2) and (3) have been solved by a fourth-order Runge–Kutta method. The schemes were combined at each time step in the following way: (i) $\theta_{H_i-1}^{n+1}$, $\theta_{H_i}^{n+1}$ and $\theta_{H_i+1}^{n+1}$ were computed writing the

kinetic terms of Eq. (1) at the previous time step n (i is a spatial discretization index); afterwards, (ii) $\theta_{O_i}^{n+1}$ and c_i^{n+1} were computed by the Runge–Kutta method (keeping the right-hand side of Eqs. (2) and (3) at the n th step). The hydrogen front speed has been calculated as the front crossed a control space interval.

3.2. Simulation results

As key experiment, we simulate the titration experiment displayed in Figs. 1 and 2. Fig. 6 displays the corresponding simulation.

The comparison of the simulated PEEM intensity during collision of reaction fronts with the experimental data in Fig. 2 demonstrates that the characteristic features of the experiment are well reproduced. The initial conditions of this 1D simulation had been chosen such that inside the island the surface is fully cov-

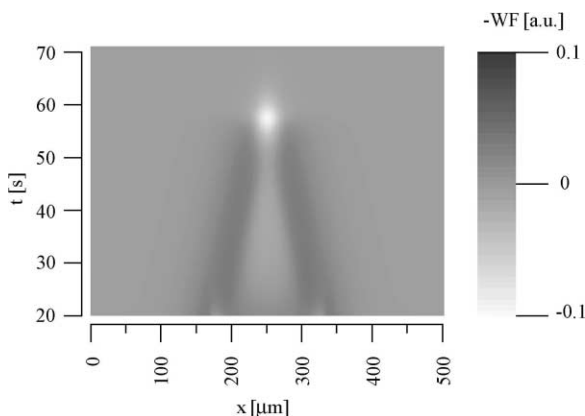


Fig. 6. Simulation of the colliding fronts. The gray-level WF image. Conditions: $p_{H_2} = 4 \times 10^{-7}$ mbar, $p_{O_2} = 3.7 \times 10^{-7}$ mbar and $T = 450$ K.

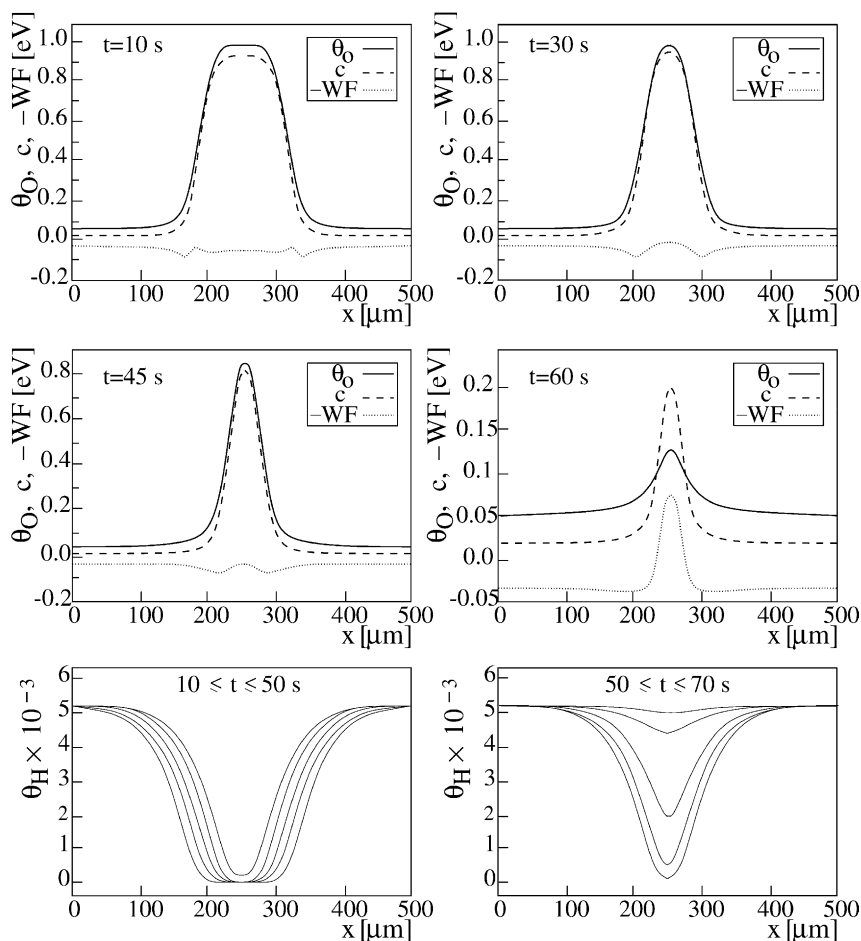


Fig. 7. Simulation of the colliding fronts: θ_O , θ_H , c and $-WF = c - \theta_O$ profiles. Conditions: $p_{\text{H}_2} = 4 \times 10^{-7}$ mbar, $p_{\text{O}_2} = 3.7 \times 10^{-7}$ mbar and $T = 450$ K.

ered with chemisorbed oxygen ($\theta_O = 1$) and that the sub-O reservoir was filled ($c = 1$). Outside the oxygen island, the adsorbate coverages had been set to zero. Exposure to H_2 leads to the reaction fronts shown in Fig. 6. The development of the adsorbate coverages during the collision is reproduced in Fig. 7.

In the reaction front, both chemisorbed oxygen and sub-O are removed because of the fast segregation of sub-O to the energetically more favorable surface sites. When the two reaction fronts have approached sufficiently, the hydrogen coverage in the area enclosed by the fronts rises and, as a consequence, the reactive removal of chemisorbed oxygen accelerates, so

that the segregation of sub-O is no longer fast enough to replace the surface oxygen which is reacted away. As a consequence, the concentration of sub-O exceeds that of chemisorbed oxygen. The contribution of the species with a negative dipole moment now dominates, and WF decreases below the level of the clean surface. The simulated WF shown in Fig. 8 can be compared with the experimental PEEM intensity WF profiles displayed in Fig. 1d. The experimental result is reproduced qualitatively in the simulation, where WF is defined as $\theta_O - c$.

Besides the main features, the simulation also reproduces details like the formation of the dark bands

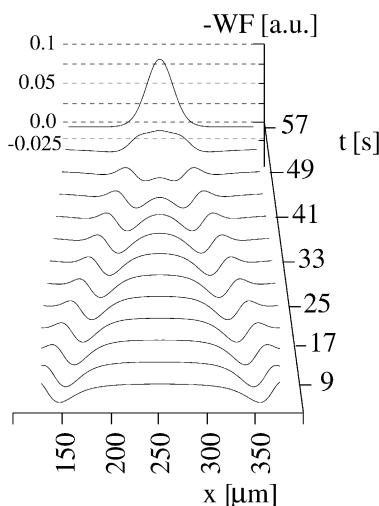


Fig. 8. Simulation of the colliding fronts: formation of low WF areas upon titration of an oxygen-covered surface with hydrogen. Conditions: $p_{\text{H}_2} = 8 \times 10^{-7}$ mbar, $p_{\text{O}_2} = 3.8 \times 10^{-7}$ mbar and $T = 530$ K.

at the reaction fronts visible in the PEEM images of Fig. 1. These dark bands only appear in the intermediate stages of the reaction. They show up as a dip in the PEEM intensity profiles of Fig. 1d. The reason for the development of the dark bands is that under certain conditions sub-O is faster removed than chemisorbed oxygen, which can be the case when segregating sub-O replaces the surface oxygen which is reacted away. A relative abundance of chemisorbed oxygen compared to the sub-O species results and the dominating contribution of the species with a positive dipole moment

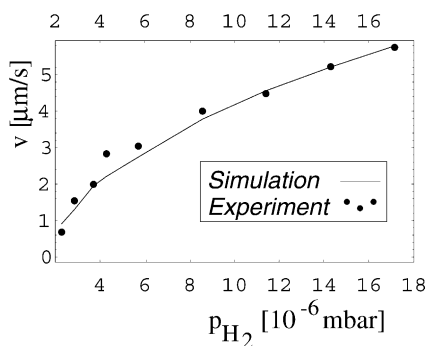


Fig. 9. The velocity of the single front motion versus p_{H_2} . Conditions: $p_{\text{O}_2} = 2.2 \times 10^{-6}$ mbar and $T = 450$ K.

leads to an increase of WF. A comparison of the calculated dependence of the front velocity on p_{H_2} with the experimental data is displayed in Fig. 9. The experimental data are well reproduced. The data follow approximately a square-root-like dependence indicating that the adsorption/desorption equilibrium of H_2 is rate-limiting for progression of the reaction fronts.

4. Conclusions and outlook

Experimentally, it has been demonstrated how the dynamics of a simple bistable surface reaction are modified when bulk oxygen becomes involved into the surface processes. Although a direct spectroscopic proof by in situ experiments for the sub-O species in these experiments is still missing, the interpretation of the LWF areas as sub-O species is consistent with all experimental data. The main obstacle in coming to a detailed mechanistic understanding of the processes which play a role here is the lack of understanding of how the transition from chemisorbed oxygen to bulk oxide formation really proceeds and what the nature of the sub-O species is. Experimentally, there are only very few techniques available with which a sub-O species can be characterized, and in any case it will be difficult to distinguish between surface, sub-surface and bulk species. A clear-cut identification of oxygen in octahedral subsurface sites on Rh(1 1 1) has been achieved by photoelectron diffraction but it might well be that this species and the species which shows up in the PEEM experiments are not identical [15]. For the formation of sub-O, a number of aspects play a role which have not been considered here explicitly. The role of adatom interactions which leads to coverage-dependent kinetic and energetic parameters has been largely neglected, in particular, the effect of high oxygen coverages which are presumably required to force the surface oxygen into subsurface sites. In the transition to a bulk oxide intermediate phases between surface oxygen and bulk oxide will probably form, and the associated change in the lattice constants will lead to elastic stress which is important for facilitating penetration of surface oxygen into bulk sites. Recent theoretical studies have begun to address these points which are also very important for understanding the so-called “pressure gap” problem in heterogeneous catalysis [25]. Here we have presented a simpli-

fied model which nevertheless is capable of reproducing a number of key observations of the experiment. Clearly, aside from the above-mentioned, mechanistic understanding, the equations need to be refined in several ways in order for the model to be more realistic. Simple Fickian diffusion for adsorbed hydrogen should be replaced by a formulation which takes into account site-blocking effects by co-adsorbates. Diffusion should follow the gradient in chemical potential to account for the changing binding strength of diffusing hydrogen. It is also evident that the change in adsorption properties on a surface with sub-O should be treated in more detail. At present, however, not enough experimental data are available to start such a project. The situation may change when quantum chemical calculations are available which provide the required kinetic and energetic parameters with some level of confidence.

Acknowledgements

This work has been supported by the German–Israeli Science Foundation. M.M and L.P. acknowledge the support by the Minerva Center for Nonlinear Physics of Complex Systems.

References

- [1] M. Eiswirth, G. Ertl, in: R. Kapral, K. Showalter (Eds.), *Chemical Waves and Patterns*, Kluwer Academic Publishers, Dordrecht, 1994.
- [2] R. Imbihl, G. Ertl, *Chem. Rev.* 95 (1995) 697.
- [3] S. Ladas, R. Imbihl, G. Ertl, *Surf. Sci.* 219 (1989) 88.
- [4] H.H. Rotermund, J. Lauterbach, G. Haas, *Appl. Phys. A* 57 (1993) 507.
- [5] J. Lauterbach, K. Asakura, H.H. Rotermund, *Surf. Sci.* 313 (1994) 52.
- [6] A.v. Oertzen, A.S. Mikhailov, H.H. Rotermund, G. Ertl, *Surf. Sci.* 350 (1996) 259.
- [7] A.v. Oertzen, A.S. Mikhailov, H.H. Rotermund, G. Ertl, *J. Phys. Chem. B* 102 (1998) 4966.
- [8] A.v. Oertzen, H.H. Rotermund, A.S. Mikhailov, G. Ertl, *J. Phys. Chem. B* 104 (2000) 3155.
- [9] N.M.H. Janssen, A. Schaak, B.E. Nieuwenhuys, R. Imbihl, *Surf. Sci.* 364 (1996) L555.
- [10] A. Schaak, Ph.D. Thesis, University of Hannover, Hannover, 1999.
- [11] A. Makeev, R. Imbihl, *J. Chem. Phys.* 113 (2000) 3854.
- [12] A. Schaak, R. Imbihl, *Chem. Phys. Lett.* 283 (1998) 386.
- [13] K.A. Peterlinz, S.J. Sibener, *Surf. Sci.* 344 (1995) L1239.
- [14] K.A. Peterlinz, S.J. Sibener, *J. Phys. Chem.* 99 (1995) 2817.
- [15] J. Wider, T. Greber, E. Wetli, T.J. Kreuz, P. Schwaller, J. Osterwalder, *Surf. Sci.* 417 (1998) 301.
- [16] P.D. Cobden, N.M.H. Janssen, Y. van Breugel, B.E. Nieuwenhuys, *Surf. Sci.* 366 (1996) 432.
- [17] P.R. Norton, *The Chemical Physics of Solid Surfaces and Heterogeneous Catalysis*, Vol. 4, Elsevier, Amsterdam, 1982, p. 27.
- [18] S. Voelkening, K. Beduerftig, K. Jacobi, J. Wintterlin, G. Ertl, *Phys. Rev. Lett.* 83 (1999) 2672.
- [19] E.G. Seebauer, A.C.F. Kong, L.D. Schmidt, *J. Chem. Phys.* 88 (1988) 6597.
- [20] S.S. Mann, T. Seto, C.J. Barnes, D.A. King, *Surf. Sci.* 261 (1992) 155.
- [21] M. Ehsasi, K. Christmann, *Surf. Sci.* 194 (1988) 172.
- [22] J.T. Yates Jr., P.A. Thiel, W.H. Weinberg, *Surf. Sci.* 84 (1979) 427.
- [23] M.L. Wagner, L.D. Schmidt, *J. Chem. Phys.* 99 (1995) 805.
- [24] A. Schaak, B. Nieuwenhuys, R. Imbihl, *Surf. Sci.* 441 (1999) 33.
- [25] K. Reuter, C. Stampfl, M. Ganduglia-Pirovano, M. Scheffler, *Phys. Rev. Lett.*, submitted for publication.